Age-Dependent Labeling and Imaging of Insulin Secretory Granules

Anna Ivanova,[1,2] Yannis Kalaidzidis,[3,4] Ronald Dirkx,[1] Mihail Sarov,[3] Michael Gerlach,[5,6] Britta Schroth-Diez,[3] Andreas Müller,[1] Yanmei Liu,[1,3] Cordula Andree,[3] Bernard Mulligan,[1,3] Carla Münster,[1] Thomas Kurth,[6] Marc Bickle,[3] Stephan Speier,[5,6] Konstantinos Anastassiadis,[6] and Michele Solimena[1,3]

Insulin is stored within the secretory granules of pancreatic β-cells, and impairment of its release is the hallmark of type 2 diabetes. Preferential exocytosis of newly synthesized insulin suggests that granule aging is a key factor influencing insulin secretion. Here, we illustrate a technology that enables the study of granule aging in insulinoma cells and β-cells of knock-in mice through the conditional and unequivocal labeling of insulin fused to the SNAP tag. This approach, which overcomes the limits encountered with previous strategies based on radiolabeling or fluorescence timer proteins, allowed us to formally demonstrate the preferential release of newly synthesized insulin and reveal that the motility of cortical granules significantly changes over time. Exploitation of this approach may enable the identification of molecular signatures associated with granule aging and unravel possible alterations of granule turnover in diabetic β-cells. Furthermore, the method is of general interest for the study of membrane traffic and aging. ***Diabetes*** **62:3687–3696, 2013**

Insulin is the key hormone for glucose homeostasis. Pancreatic β-cells produce insulin and store it within secretory granules (SGs) until elevated glycemia triggers SG exocytosis and insulin release. Seminal studies using pulse-chase labeling protocols indicated that newly synthesized insulin is preferentially released (1,2). Until today, however, a method for the reliable imaging and study of age-distinct insulin SGs has not been available. In this article, we present a new approach that enables the unequivocal imaging and study of insulin SGs of defined age.

RESEARCH DESIGN AND METHODS

Constructs. The human preproinsulin cDNA was cloned in frame with the *SNAP* tag either into *pEGFP-N1* (Clontech) void of the *GFP* cDNA or into the *pShuttle-CMV* vector (Qbiogene). The adenoviral construct *pAdEAsy-1-RIP-hIns-SNAP* was transfected into QBI-293A cells (Qbiogene) to produce adenovirus *RIP-hIns-SNAP*. For generation of the SOFIA (Study OF Insulin granule Aging) mouse, the *SNAP* cDNA was subcloned into a vector carrying the neoresistance gene, driven by *PGK/gb3* promoter and flanked by flippase recognition target sites (oligos: *CCAATGCATTGGTTCTGCAGTTTGGGATCCACCGGTC*, *GAAGATCTTCGGACTAGTCCCTAACCCAGCCCAGG*). This plasmid was used to generate a bacterial artificial chromosome tagging cassette (oligos: *CAGTGCTGCACCAGCATCTGCTCCCTCTACCAGCTGGAGAACTACTGCAACTGGGATCCACCGGTCGCCACCGAG*, *CTCATTCAAAGGTTTTATTCATTGCAGAGGGGTAGGCTGGGTAGTGGTGGGTCTATCCAAGACCCCGACGTGTGCTCAC*), which was used for Red-ET recombineering as previously described (3). All constructs were verified by sequencing.

Islet isolation and cell culture. Islets from SOFIA and control C57Bl/6J mice were isolated and cultured as previously described (4). INS-1 and MIN6 cells were kind gifts from Claes Wolheim (Geneva, Switzerland) and Jun-ichi Miyazaki (Osaka, Japan) and were grown as described (5,6).

Cell transfection and transduction. INS-1 and MIN6 cells were transiently transfected with pEG-hIns-SNAP or the *insulin2-SNAP-PGK-neo* bacterial artificial chromosome, respectively, as previously described (7). Islet cells were transduced with adenovirus *RIP-hIns-SNAP*.

Generation of the SOFIA mouse. Mouse JM8.F6 (C57Bl/6N) embryonic stem (mES) cells were cultured on mitomycin-C inactivated mouse embryonic fibroblasts (MEFs) using embroyonic stem cells (ESs) medium containing leukemia inhibitory factor. mES cells (1×10^7) were electroporated with 40 μg linearized *insulin2-SNAP-PGK-neo* construct using 250 V (Bio-Rad) and selected with 200 μg/mL G418 (Invitrogen). Colonies were screened by Southern hybridization using a 5′-external probe (*Spe*I) or a 3′-external probe (BsrGI/MunI) and an internal probe (neo) using BsrGI/MunI. *Insulin2-SNAP-PGK-neo* mES cells were injected into C57Bl6 blastocysts (Transgenic Core Facility, Max Planck Institute for Molecular Cell Biology and Genetics, Dresden, Germany). Chimaeras were crossed to Bl6 mice, and the progeny was genotyped. Positive mice were further crossed with a Flpo-expressing mouse strain (8).

Measurement of TMR-Star$^+$-hIns-SNAP secretion. Secretion of Ins-SNAP-TMR-Star was measured in stable *hIns-SNAP* INS-1 cell clones 8 (expresses hIns-SNAP) and 5 (no detectable hIns-SNAP) seeded either in 12-well (2.33×10^5 cells/well) or 384-well (3.5×10^4 cells/well) plates. The latter clone was used to subtract background fluorescence. The cells were sequentially incubated in *1*) 25 mmol/L glucose and 55 mmol/L KCl HEPES buffer (15 mmol/L HEPES, pH 7.4; 70 mmol/L NaCl; 24 mmol/L $NaHCO_3$; 1 mmol/L $MgCl_2$; 2 mmol/L $CaCl_2$; and 1 mg/mL albumin) for 1 h; *2*) RPMI 1640 with 2.8 mmol/L glucose and 20 μmol/L BTP (blocking SNAP substrate) for 20 min; *3*) RPMI 1640 for 3 h; *4*) RPMI 1640 with 0.8 μmol/L TMR-Star for 45 min; *5*) RPMI 1640 for 1–20 h; *6*) 0 mmol/L glucose and 5 mmol/L KCl in HEPES buffer with 120 mmol/L NaCl for 1 h; and *7*) 0 mmol/L glucose, 5 mmol/L KCl or 25 mmol/L glucose, and 55 mmol/L KCl in HEPES with 120 mmol/L NaCl for 1 h. Media from resting and stimulated *hIns-SNAP* INS-1 cells and the corresponding cell extracts were scanned with an EnVision reader (Perkin Elmer).

Radioimmunoassays. Human insulin, human C-peptide, human proinsulin, and rat insulin were measured by radioimmunoassay (RIA) according to the manufacturer's recommendations (Linco Research). Cells were kept at rest or stimulated as described above.

Subcellular fractionation. Transiently transfected *hIns-SNAP* INS-1 cells were processed as previously described (7).

Western blotting. Total protein extracts or subcellular fractions of *hIns-SNAP* INS-1 cells and SOFIA mouse islets were immunoblotted with anti-insulin (Sigma), anti–A-chain (Santa Cruz), anti-CPE (Chemicon), anti–GM-130 (BD Biosciences), and anti–γ-tubulin (Sigma) antibodies.

In vitro labeling of cultured cells with SNAP substrates for imaging studies. All labeling steps were carried out in RPMI 1640 with 11 mmol/L glucose unless otherwise stated. Single labeling of transiently transfected *hIns-SNAP* INS-1 cells and *insulin2-SNAP-PGK-neo* MIN6 cells for confocal microscopy involved the following incubation steps: *1*) 0.8 μmol/L TMR-Star (New England Biolabs) or 10 μmol/L BG-505 (New England Biolabs) for

From [1]Molecular Diabetology, Paul Langerhans Institute Dresden, Dresden University of Technology, Dresden, Germany; the [2]International Max Planck Research School, Dresden, Germany; the [3]Max Planck Institute of Molecular Cell Biology and Genetics, Dresden, Germany; the [4]A.N. Belozersky Institute of Physico-Chemical Biology, Moscow State University, Moscow, Russia; [5]Islet Cell Regeneration, Paul Langerhans Institute Dresden, Dresden University of Technology, Dresden, Germany; and the [6]Center for Regenerative Therapies Dresden, Dresden University of Technology, Dresden, Germany.
Corresponding author: Michele Solimena, michele.solimena@tu-dresden.de.
Received 2 January 2013 and accepted 17 July 2013.
DOI: 10.2337/db12-1819
This article contains Supplementary Data online at http://diabetes.diabetesjournals.org/lookup/suppl/doi:10.2337/db12-1819/-/DC1.

30 min, *2*) RPMI 1640 for 30 min, and *3*) 4% paraformaldehyde (PFA) in PBS. Double labeling of *hIns-SNAP* INS-1 cells for confocal and total internal reflection fluorescence (TIRF) microscopy involved the following steps: *1*) 0.8 μmol/L TMR-Star for 15 min, *2*) RPMI 1640 for 30 min, *3*) 11 μmol/L BTP in DMSO or DMSO alone for 20 min, *4*) RPMI 1640 for 4 h, *5*) 10 μmol/L BG-505 for 30 min, *6*) RPMI 1640 for 30 min, and *7*) 4% PFA in PBS. For TIRF microscopy, the last step was omitted. Alternatively, *hIns-SNAP* INS-1 cells were double labeled for confocal microscopy as follows: *1*) 11 μmol/L BTP for 20 min, *2*) RPMI 1640 for 2 h, *3*) 0.8 μmol/L TMR-Star for 15 min, *4*) 11 μmol/L BTP for 20 min, *5*) RPMI 1640 for 2 h, *6*) 10 μmol/L BG-505 for 30 min, *7*) RPMI 1640 for 30, and *8*) 4% PFA in PBS. Single labeling of *hIns-SNAP* INS-1 cells for TIRF microscopy involved the following steps: *1*) HEPES with low glucose (2.8 mmol/L) and high KCl (55 mmol/L) (LGHP) and 70 mmol/L NaCl for 30 min, *2*) HEPES LGHP with 20 μmol/L BTP for 30 min, *3*) HEPES with 250 μmol/L diaxozide for 2 h, *4*) HEPES with 250 μmol/L diaxozide and 0.8 μmol/L TMR-Star or 18.5 μmol/L BG-505 for 45 min, and *5*) HEPES with 2.8 mmol/L glucose and 5 mmol/L KCl buffer for 1.5–4.5 h. In some instances, cells were fixed with 4% PFA in PBS while imaging. *hIns-SNAP* INS-1 cells cultured in 384-well plates (3.5×10^4 cells/well; Aurora) were labeled as follows: *1*) HEPES LGHP for 30 min; *2*) HEPES LGHP with 20 μmol/L BTP for 30 min; *3*) RPMI 1640 for 90 min; *4*) 0.8 μmol/L TMR-Star for 45 min; *5*) HEPES with 5 mmol/L glucose and 5 mmol/L KCl for 90 min; *6*) HEPES with 25 mmol/L glucose, 55 KCl, or 5 mmol/L glucose and 5 mmol/L KCl for 60 min; and *7*) 3.5% PFA in PBS.

In vivo labeling of Ins-SNAP in mice with SNAP substrates for imaging studies. SOFIA and C57Bl/6J mice were administered 15 nmol TMR-Star via tail vein injection. After 30 min–2 h, pancreata were explanted and processed in one of the following ways: *1*) fixed with 4% PFA for cryosectioning and immunostaining, *2*) digested with collagenase for islet isolation, or *3*) perfused with agarose for vibratome sectioning as previously described (9).

Immunocytochemistry. *INS*-1 cells, *hIns-SNAP* INS-1 cells, *insulin2-SNAP-PGK-neo* MIN6 cells, and pancreatic cryosections of SOFIA mice were immunolabeled using the following antibodies: anti-insulin (DAKO), anti-CgA (BD Biosciences), anti-TGN (BD Biosciences), anti-EEA1 (BD Biosciences), anti-GM130 (BD Biosciences), anti-PDI (Stressgen Biotechnologies), anti-glucagon (Sigma), and anti-somatostatin (US Biomax).

Confocal microscopy. TMR-Star–labeled *hIns-SNAP* INS-1 cells, *insulin2-SNAP-PGK-neo* MIN6 cells, and pancreatic cryosections were imaged with a CLSM Zeiss LSM 510 equipped with 488 nm, 561 nm lasers; Plan-APOCHROMAT 63×/1.4 oil; HFT 405/488/561; BP505-530; and LP575.

For in situ imaging of islets, in vibratome sections LSM780 CM (Zeiss) equipped with a 20×/1.0 objective was used. Tissue backscatter was recorded by detecting reflection of the 405-nm laser at 395–415 nm. Imaris 7.4 was used for image processing. For increase of contrast, linear stretch was applied to all images. High-magnification images were deconvolved using blind deconvolution algorithm (AutoQuant). Confocal images of labeled *hIns-SNAP* INS-1 cells in 384-well plates were acquired with a Perkin Elmer OPERA at ×60.

TIRF microscopy. The data in Fig. 4*A*, *C*, and *D* were acquired with an Olympus IX-71–based TIRF system with UApo150×/1.45 NA, BLHC617/73 (Semrock), and iXon+DU897 (0.106 μm/pixel) (AndorTechnology). For dual color (Supplementary Movie 1), a 100×/1.45 NA Oil (0.164 μm/pixel) objective was used. The remainder data were acquired using a NikonEclipse-Ti microscope, with 2 iXon+ DU897, 100×/1.49 Apo TIRF (0.161 μm/pixel), BP512/18, and BP647/57 (Semrock).

Light-sheet microscopy. SOFIA islets labeled in vivo for 2 h by TMR-Star injection were isolated, fixed with 4% PFA, and imaged with an LSF Microscope (Zeiss) equipped with a 561-nm laser, LBF405/488/561, and W PlanApochromat 63×/1.0.

Immunoelectron microscopy. *hIns-SNAP* INS-1 cells and SOFIA islets were processed for Tokuyasu cryosectioning and immunolabeling as previously described (10–12) using mouse anti-SNAP (Chemicon), guinea pig anti-insulin (Abcam), and rabbit anti-mouse (bridging antibody; Sigma) antibodies followed by protein A conjugated to 10-nm or 15-nm gold particles (Aurion).

Imaging and statistical analyses. All confocal images, unless otherwise stated, were analyzed with the Fiji software plug-ins "colocalization threshold" and "colocalization test" and subjected to the Costes colocalization significance test (13). Segmentation analysis of insulin$^+$, CgA$^+$, and TMR-Star$^+$ objects in immunolabeled INS-1 and *hIns-SNAP* INS-1 cells was carried out with CellProfiler. Cells with <20 fluorescent objects and objects with fewer than three pixels, i.e., not fulfilling Nyquist's sampling requirement, were excluded from the analysis. Binary masks of all objects were measured for surface overlap. Threshold for object colocalization was an overlap ≥30%. TIRF data were analyzed using MotionTracking (14,15), which allows for the identification of single objects and their tracking through the dataset. All tracks with a minimum length of 10 frames (frame rate ~30 frames per second) were considered. The processivity criteria required that the tracks indicate unidirectional transport for at least four frames with maximum deviation of 30°. We analyzed 6,920, 4,405, 4,244, and 4,800 tracks for the 2–4 h (18 movies), 3–5 h (10 movies), 4–6 h (16 movies), and 5–7 h (26 movies) time points, respectively. The decay of the TMR-SNAP$^+$-SG mean speed was found by fitting a straight line by maximum-likelihood estimation. The fitting was done with the Pluk mathematical library (16). The statistical significance was assessed by a two-tailed Student *t* test. The statistical significance of the immunoelectron microscopy data was assessed by a two-tailed Student *t* test. Images of labeled *hIns-SNAP* INS-1 cells in 384-well plates were analyzed with CellProfiler.

RESULTS

Generation and expression of human insulin-SNAP. To image age-distinct pools of insulin SGs, we tagged human insulin with SNAP (hIns-SNAP) (Fig. 1*A*) and transiently expressed it in rat insulinoma INS-1 cells (*hIns-SNAP* INS-1 cells). SNAP is a 22-kDa polypeptide derived from human O6-alkylguanine-DNA alkyltransferase (AGT), a suicidal enzyme involved in DNA repair. For generation of SNAP, AGT was modified such that its catalytic cysteine covalently binds benzylguanine-containing substrates while having lost DNA-binding capability (17–19). Cell-permeable fluorescent SNAP substrates include TMR-Star and BG-505. Immunoblotting of *hIns-SNAP* INS-1 cell lysates with an anti-insulin antibody detected a ~31 kDa protein, as expected for proinsulin-SNAP (hProIns-SNAP [Fig. 1*B*]). An anti-human A-chain antibody detected an additional ~24 kDa protein, as expected for A-chain SNAP (Fig. 1*B*). Both antibodies reacted with neither non-transfected INS-1 cell lysates nor purified His-tagged SNAP, while endogenous rat proinsulin (~11 kDa) and insulin A-chain (~2 kDa) were outside the size resolution range of these gels.

Immunoblot quantifications indicated that in *hIns-SNAP* INS-1 cells incubated with 2.8 mmol/L glucose, the mean rat insulin–to–hIns-SNAP ratio was 1.12 ± 0.33 (n = 3), while hProIns-SNAP–to–hIns-SNAP ratio was 2.02 ± 0.18 (n = 3) (Fig. 1*C*). Stimulation of *hIns-SNAP* INS-1 cells with 11 mmol/L glucose increased the hProIns-SNAP–to–hIns-SNAP ratio to 8.61 ± 2.55 (n = 3), mainly because the content of hIns-SNAP, similarly to endogenous insulin, was diminished, conceivably due to its release. Comparable changes were observed with the anti-A chain antibody (Supplementary Fig. 1). Hence, INS-1 cells express hProIns-SNAP and convert it into hIns-SNAP, albeit less efficiently than endogenous proinsulin.

hIns-SNAP is targeted to and released from insulin granules. Conversion of hProIns-SNAP suggests its sorting into SGs (20,21). By confocal microscopy, TMR-Star$^+$-hProIns-SNAP/hIns-SNAP appeared concentrated in cytosolic puncta, which were also positive for the SG marker chromogranin A (CgA) (22) (Fig. 2*A*). Spatial intensity correlation analysis (13,23) indicated a Pearson correlation coefficient (Rcoloc) for TMR-Star$^+$-hIns-SNAP and CgA of 0.76 ± 0.05 (n = 13 cells), with thresholded Manders coefficients being $tM1_{avg}$ = 0.91 ± 0.05 and $tM2_{avg}$ = 0.95 ± 0.05 (controls, $Rcoloc_{avg}$ = 0.72 ± 0.04, $tM1_{avg}$ = 0.53 ± 0.06, and $tM2_{avg}$ = 0.81 ± 0.06). Colocalization of TMR-Star$^+$-hIns-SNAP with SGs was further supported by segmentation analysis, which showed that 80.3 ± 3.6% of insulin$^+$ objects (controls, 100%) and 70.4 ± 12.7% of TMR-Star$^+$ hIns-SNAP objects (87.71% of controls) were also CgA$^+$. Furthermore, TMR-Star$^+$-hIns-SNAP did not colocalize with markers of the endoplasmic reticulum, the *trans*-Golgi network, or early endosomes (Supplementary Figs. 2–4).

Next, we assessed the localization of hIns-SNAP by cryoimmunoelectron microscopy. Immunostaining for SNAP alone or together with insulin showed their specific colocalization in SGs, with equivalent background levels

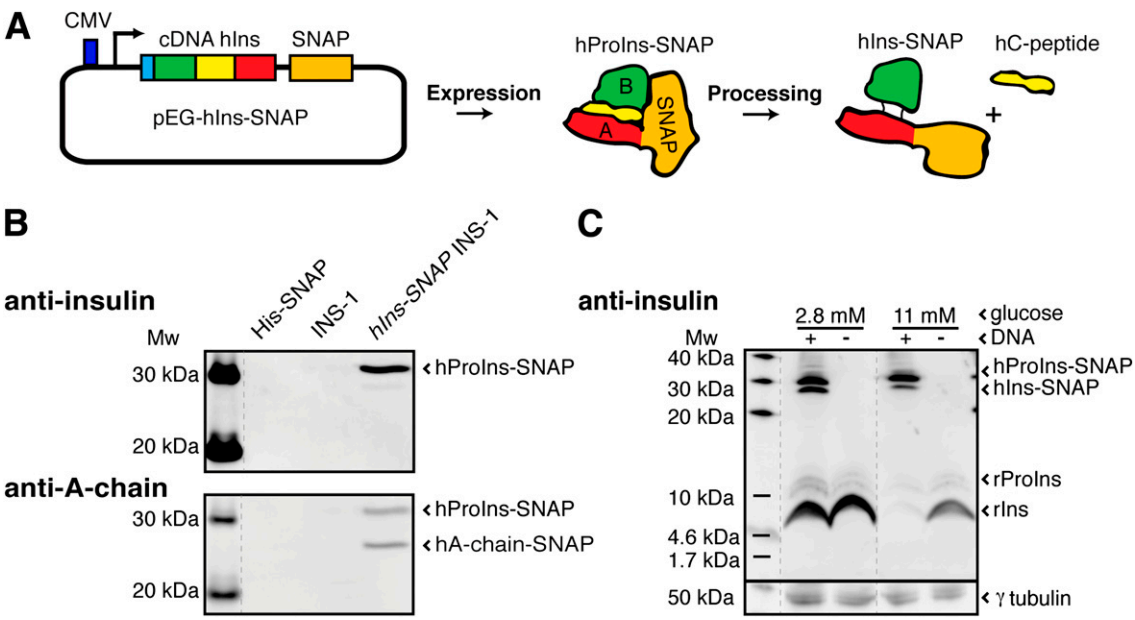

FIG. 1. hIns-SNAP is expressed and converted in INS-1 cells. *A*: pEG-hIns-SNAP construct. Vector for the expression of human preproinsulin fused to SNAP. Mature hIns-SNAP includes the B-chain and A-chain SNAP connected by disulfide bridges. Dark blue, cytomegalovirus promoter (CMV); light blue, signal peptide; green, B-chain; yellow, C-peptide; red, A-chain; orange, SNAP. *B*: Expression of hIns-SNAP in INS-1 cells. Immunoblotting with anti-insulin (*upper panel*) and anti–A-chain (*lower panel*) antibodies on purified recombinant His-SNAP and reduced lysates of transiently transfected *hIns-SNAP* INS1-cells or nontransfected INS-1 cells separated by SDS-PAGE. A dotted line indicates where the image of the original blot was cut to assemble the figure. *C*: Expression of hIns-SNAP and rat insulin in INS-1 cells. Immunoblotting with anti-insulin (*upper panel*) and anti–γ-tubulin (*lower panel*) antibodies on nonreduced lysates of transiently transfected *hIns-SNAP* INS1-cells (+) or nontransfected (-) and incubated with 2.8 or 11 mmol/L glucose prior to extraction and separation on a Tris-tricine gel. Dotted lines indicate where images of the original blot were cut to assemble the figure. *B* and *C* are representative results of three independent experiments. Mw, molecular weight markers.

for both proteins in the cytosol, mitochondria, and nuclei (Fig. 2*B* and Table 1).

Finally, we analyzed the intracellular distribution of hIns-SNAP in subcellular fractions of transiently transfected *hIns-SNAP* INS-1 cells (Fig. 2*C*). One peak of hProIns-SNAP was detected in lighter fractions enriched in the Golgi marker GM130. Another peak was present in heavier fractions, which were also enriched for the 54 kDa form of carboxypeptidase E, a marker of mature insulin SGs (24). These fractions were also enriched in hA-chain-SNAP, although hProIns-SNAP remained the prevalent form.

Being sorted into SGs, hIns-SNAP should be released in a regulated fashion. We measured with RIA the static secretion of hIns-SNAP, hProIns-SNAP, human C-peptide, and rat insulin from *hIns-SNAP* INS-1 cells stimulated with 25 mmol/L glucose and 55 mmol/L KCl for 1 h (n = 3). The RIA for human insulin had negligible cross-reactivity toward rat insulin and human proinsulin (25), while the RIA for human C-peptide does not detect rat C-peptide. Stimulation triggered the release of hIns-SNAP, hProIns-SNAP, and human C-peptide (Fig. 2*D* and *E* and Table 2), indicating that INS-1 cells corelease hProIns-SNAP, hIns-SNAP, and hC-peptide with endogenous insulin in a regulated fashion, although a large fraction of hProIns-SNAP had not been converted into hIns-SNAP.

Pulse-labeling experiments (1,2) could not distinguish between bona fide preferential release of newer insulin versus heterogeneity among β-cells, with those cells displaying faster insulin turnover being labeled to a greater extent during the pulse and then preferentially secreting during the chase. To address this question, we plated *hIns-SNAP* INS-1 cells in 384-well plates and counted 3–4 h ± 30-min-old TMR-Star$^+$ SGs by confocal microscopy. We counted 2,616,149 TMR-Star$^+$ SGs in 33,795 resting cells (median 70 ± 40 median absolute deviation/cell) vs. 1,212,080 TMR-Star$^+$ SGs in 24,262 stimulated cells (median 44 ± 31 median absolute deviation/cell) (Fig. 2*G* and *H*). The data were log normalized to obtain a nearly normal distribution (Fig. 2*G*), while its location was normalized by dividing the median of each population (Fig. 2*F*). A Kolmogorov-Smirnov two-tailed test was repeated 10 times on a sample of 100 data points drawn randomly from each population. The statistics were consistent with the populations being drawn from the same distribution (average D = 0.14, average P = 0.36 at α = 0.05). These results are consistent with the hypothesis of the secretory response being homogenous over the entire cell population rather than being primarily sustained by a more active subpopulation.

Unequivocal imaging of age-defined and -distinct insulin granule pools. Next, two age-distinct SG pools were labeled in the same cells using a protocol including three main steps (Fig. 3*A* and *B*). First, transiently transfected *hIns-SNAP* INS-1 cells were incubated with TMR-Star for 15 min to label hProIns-SNAP/hIns-SNAP expressed in the cells at that time. Second, 10 μmol/L BTP was added for 20 min to block any unlabeled hIns-SNAP. Third, cells were cultured for 4 h to allow for the synthesis of new SGs, which were then labeled with BG-505 for 30 min. The longer incubation with BG-505 was devised to compensate for its lower brightness compared with TMR-Star (18). After washes, the cells were either fixed or imaged live by TIRF microscopy. Hence, TMR-Star$^+$ SGs were "older" than 5 h and 20 min, while BG-505$^+$ SGs were younger than 5 h (Fig. 3*A* and *B* and Supplementary Movie 1). BG505$^+$ SGs were spatially segregated from TMR-Star$^+$ SGs ($Rcoloc_{avg}$ = 0.45 ± 0.11, n = 10 cells) (Fig. 3*A*). If the intervening BTP

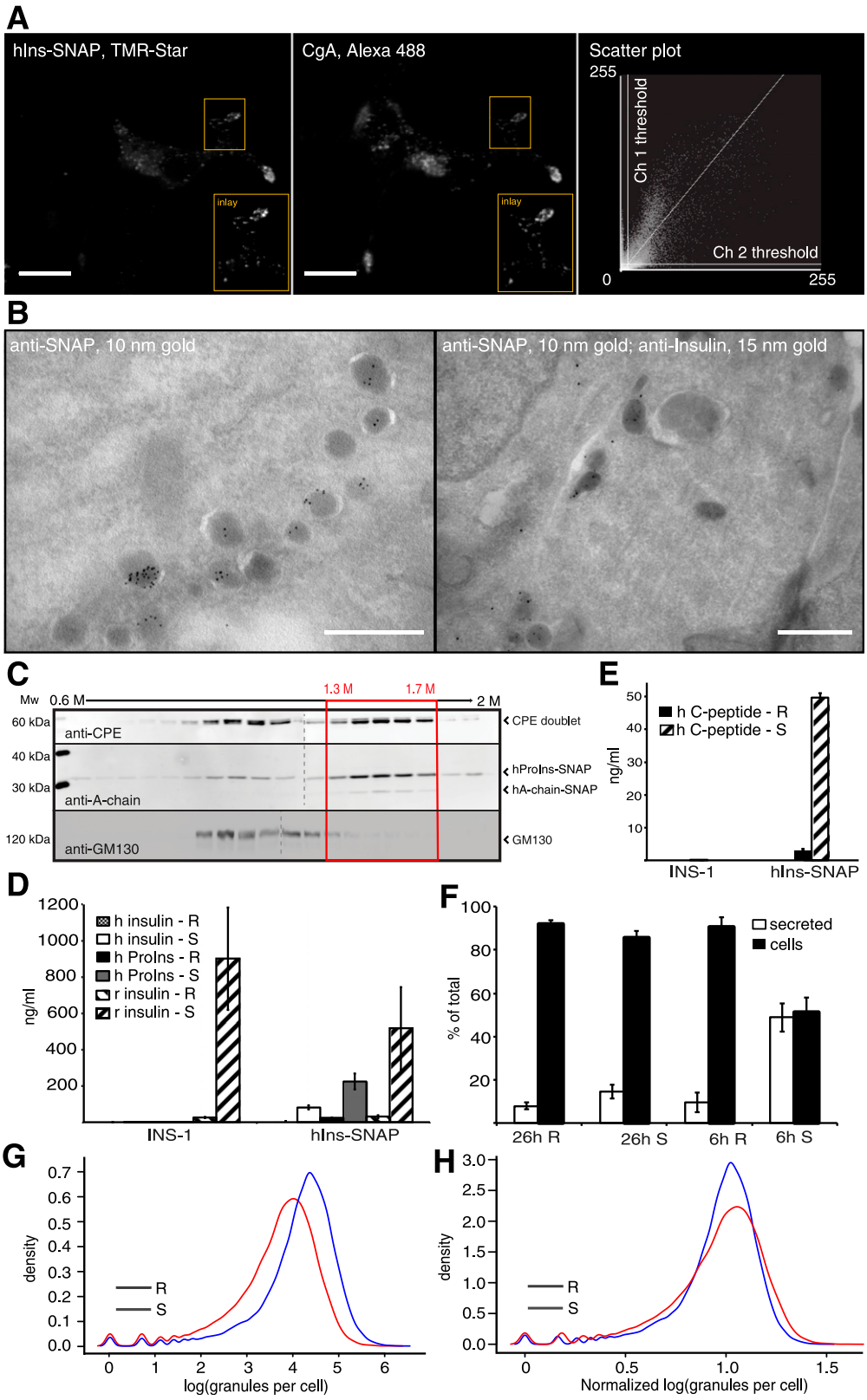

FIG. 2. Sorting of hIns-SNAP into insulin SGs and preferential release of newly synthesized hIns-SNAP. *A*: Confocal immunomicroscopy. Transiently transfected *hIns-SNAP* INS-1 cells were labeled with TMR-Star and coimmunostained after fixation for CgA. The *insets* show cytoplasmic extensions, where SGs accumulate. Scale bar: 10 μm. The scatter plot in the *right panel* shows the pixel-intensity distribution of the signals for TMR-Star (*y*-axis) and CgA (*x*-axis). *B*: Cryoimmunoelectronmicroscopy. Cryosections of transiently transfected *hIns-SNAP* INS-1 cells immunogold labeled for SNAP (*left panel*) or double immunogold labeled for SNAP and insulin (*right panel*). Scale bar: 500 nm. *C*: Subcellular fractionation. Immunoblotting on subcellular fractions of transiently transfected *hIns-SNAP* INS-1 cells cultured in 11 mmol/L glucose and separated on sucrose density gradients. The fractions from the subcellular fractionation were loaded on two gels, separated by a dividing line. *D*: RIA for human insulin and proinsulin and rat insulin. Concentrations of human insulin and proinsulin and rat insulin in the media of resting (R) (0 mmol/L glucose and 5 mmol/L KCl in HEPES buffer with 120 mmol/L NaCl) and stimulated (S) (25 mmol/L glucose and 55 mmol/L KCl in HEPES with 120 mmol/L NaCl)

TABLE 1
Quantification of immunoelectron microscopy

Labeling	Anti-SNAP (single)	Anti-SNAP (double)	Anti-insulin (double)
No. of cells	11	14	14
SGs (gp/m^2)	812.7	47.4	261.2
Background (gp/μm^2)	1.2	0.2	1.8
P	0.000948	0.002068	0.0000026

Single (anti-SNAP antibody) and double (anti-SNAP and anti-insulin antibodies) immunostaining of *hIns-SNAP* INS-1 cells was performed on cryosections. Dual labelings for insulin and SNAP were performed consecutively. gp, number of gold particles.

TABLE 2
Summary of RIA results

RIA specificity	Resting (ng/mL)	Stimulation (ng/mL)
Human insulin (*hIns-SNAP* INS-1 cells)	6.21 ± 1.21	81.75. ± 11.73
Human proinsulin (*hIns-SNAP* INS-1 cells)	25.53 ± 3.08	221.31 ± 31.20
Rat insulin (*hIns-SNAP* INS-1 cells)	30.54 ± 8.59	517.11 ± 227.33
Rat insulin (INS-1 cells)	26.19 ± 3.29	900.96 ± 282.61
Human C-peptide (*hIns-SNAP* INS-1 cells)	3.02 ± 0.76	49.77 ± 7.93

Human insulin, human proinsulin, rat insulin, and human C-peptide were measured by RIA. A set for measurements consisted of one well (in triplicate) of cells incubated in resting and one well (in triplicate) in stimulation conditions (n = 3).

blocking step was omitted, BG-505 and TMR-Star signals considerably overlapped (Pearson correlation coefficient$_{average}$ = 0.70 ± 0.05, n = 7 cells) (Fig. 3*B*). Addition of BTP prior to labeling with the first fluorophore allows the time resolution of older SGs to be restricted and defined more accurately. More younger and fewer older SGs were observed when TMR-Star and BG-505 were applied in the reverse order (Supplementary Fig. 5), reflecting differences between the two dyes with respect to brightness, photostability, and membrane permeability (18). Hence, for quantitative analysis of age-distinct SG pools, we opted to label separate samples with the same SNAP fluorophore and vary the time interval between the "pulse" and "chase" labeling.

We assessed the release of TMR-Star$^+$ hIns-SNAP from younger and older SGs by fluorimetry. Resting cells secreted comparable amounts of 4- to 6-h-old (9.0%) and 24- to 26-h-old (6.4%) TMR-Star$^+$ hIns-SNAP (Fig. 2*F*). Upon stimulation with 25 mmol/L glucose and 55 mmol/L KCl, however, only 11.0% of 24- to 26-h-old TMR-Star$^+$ hIns-SNAP was released compared with 50.6% of 4- to 6-h-old TMR-Star$^+$ hIns-SNAP (n = 3). These data are consistent with newly synthesized insulin being preferentially released (1,2). The release of 4- to 6-h-old TMR-Star$^+$ hINS-SNAP from *hIns-SNAP* INS-1 cells in 384-well plates could be independently measured by fluorimetry (Supplementary Fig. 6). These data, which are consistent with the ~40% reduction in the number of 3- to 4-h ± 30 min TMR-Star$^+$ SGs measured in stimulated *hIns-SNAP* INS-1 cells by automated microscopy (Fig. 2*G* and *H*), indicate that the sensitivity of this approach is suitable for large-scale screenings.

Age-distinct insulin granules differ in their mobility and processivity. Next, we tracked the motility of age-distinct SGs by TIRF microscopy. In *hIns-SNAP* INS-1 cells exposed to 2.8 mmol/L glucose, the mean speed of processive SGs at the cell cortex steadily decreased with time (Fig. 4*A*, Table 3, and Supplementary Movies 2 and 3 for 2- to 4-h-old and 5- to 7-h-old TMR-Star$^+$ SGs, respectively) (for processivity criteria, see IMAGING AND STATISTICAL ANALYSES). Decreased motility of processive SGs was accompanied by reduction of their track maximum displacement (defined as the distance between the two furthest points within a SG trajectory [Fig. 4*B*]), indicating that their processive transport is age-dependent (Fig. 4*C* and Table 3). We further correlated the mean speed of age-distinct processive SGs with their fluorescence intensity (Fig. 4*D*). Processive SGs brighter than 1,100 arbitrary units (AU), conceivably the closest to the plasma membrane, displayed the lowest mean speed regardless of their age, suggesting that SGs in proximity of the cell surface, within the analyzed age window, are similarly restrained. Conversely, for SGs with brightness <1,100 AU, the lower the intensity, the higher the mean speed. Still, age-distinct SGs of comparable brightness differed in their motility, with the youngest being the fastest. Hence, SG processivity depends not only on restraints imposed by the surrounding environment but also on changes inherent to their aging. The molecular mechanisms underlying these differences remain to be uncovered.

Targeting of Ins-SNAP into mouse islets in vitro and in vivo. The suitability of this technology was further tested by targeting insulin-SNAP into mouse islets in vitro and in vivo. For the first aim, we transduced mouse islets with a hIns-SNAP adenoviral vector (Fig. 5*A.1* and *B* and Supplementary Movie 4). For the second aim, we generated the SOFIA mouse, in which one *Ins2* locus was targeted with a mouse *Ins2-SNAP* cassette (Fig. 5*A.2*), previously validated in transfected mouse MIN6 cells (Supplementary Fig. 7).

The correct integration of *mIns2-SNAP* in the chosen ES clone was verified by Southern blotting (Supplementary Fig. 8), while the progeny of chimeric mice generated with this clone was genotyped by PCR. Immunoblottings for insulin on nonreduced islet extracts indicated that SOFIA mouse islets expressed both mProIns2-SNAP and mIns2-SNAP (Fig. 5*C*). The mProIns2-SNAP–to–mIns2-SNAP and insulin–to–mIns2-SNAP ratios were 1.36 ± 0.12 and 1.92 ± 0.64, respectively, whereas the insulin ratio

transiently transfected *hIns-SNAP* INS-1 cells and control INS-1 cells for 1 h (n = 3). y-axis: ng/mL. *E*: RIA for human C-peptide. Concentrations of human C-peptide in the media of resting and stimulated transiently transfected *hIns-SNAP* INS-1 cells and control INS-1 cells (n = 3). y-axis: ng/mL. *F*: Release of age-distinct hIns-SNAP pools. Percentages of the total amount of 4- to 6-h and 24- to 26-h-old TMR-Star$^+$ hIns-SNAP in the media and extracts of resting or stimulated INS-1 cells stably expressing hIns-SNAP, as measured by fluorimetry (n = 3). y-axis: % of total. *G*: Release of hIns-SNAP 384-well plate format. Log transformation of the granule distribution data in resting cells (R) (2.8 mmol/L glucose and 5 mmol/L KCl in HEPES buffer with 120 mmol/L NaCl) or upon stimulation (S) (as in *D*). y-axis: estimation of the probability. *H*: Normalization of the data presented in Fig. 2*H*. CPE, carboxypeptidase E; GM130, Golgi matrix protein of 130 kDa.

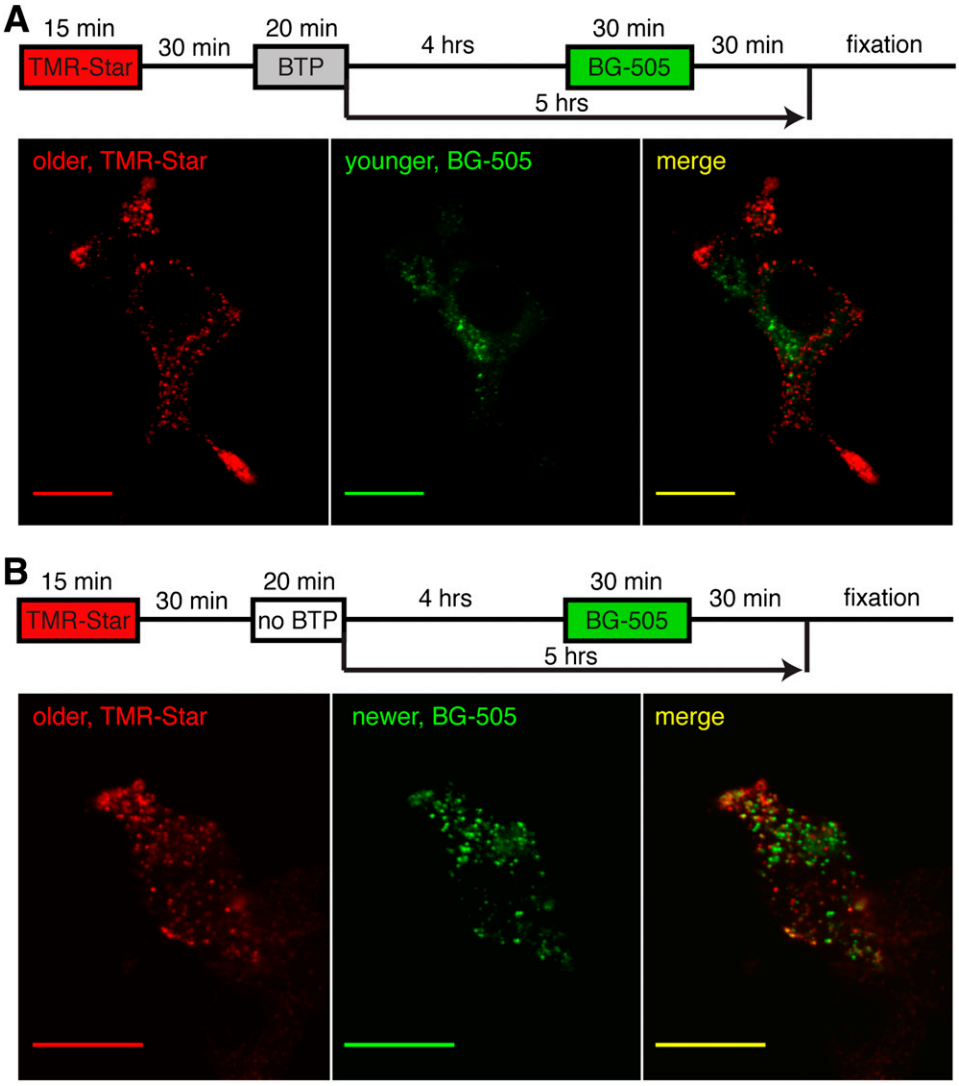

FIG. 3. Simultaneous detection of age-distinct insulin SGs. *A* and *B*: Confocal microscopy. Transiently transfected *hIns-SNAP* INS-1 cells were sequentially labeled with TMR-Star and BG-505 according to the indicated schemes. In *A*, but not in *B*, cells were incubated with the nonfluorescent SNAP substrate BTP (block) before being incubated with BG-505. Scale bar: 10 μm. Hrs, hours.

between SOFIA and C57Bl/6 islets was 0.12 ± 0.06 (n = 3). The sorting of mIns2-SNAP in SGs was verified by cryo-immunoelectron microscopy (Fig. 5*D* and Supplementary Table 1). Next, we attempted the labeling of mIns2-SNAP in vivo. For this, pancreatic tissue slices and sections of SOFIA mice were prepared 30–120 min after intracardiac or intravenous injection of TMR-Star. The SNAP labeling was restricted to islets (Fig. 5*E*) and specifically to β-cells, as α- and δ-cells (Fig. 5*F* and Supplementary Fig. 9) were TMR-Star^{-}. Notably, 30 min after TMR-Star injection the fluorescence was mostly perinuclear (Fig. 5*F*), while after 2 h it was mostly granular and scattered throughout the cells (Fig. 5*E*), consistent with the temporal progression of mProIns2-SNAP/mIns2-SNAP from the Golgi complex to SGs, as reported for $^{[3H]}$proinsulin/insulin in isolated islets in vitro (26). The TMR-Star signal was retained even after SOFIA islets labeled in vivo by tail vein injection had been isolated by collagenase digestion (Fig. 5*G*).

DISCUSSION

The functional heterogeneity and turnover of insulin SGs in relation to their spatial and age distribution deserve greater attention, as knowledge about the molecular basis of such heterogeneity could be relevant for the understanding and treatment of type 2 diabetes. Hallmarks of the disease onset are a blunted first phase of insulin secretion and an increased proinsulin release (27). In the prevailing model, insulin SGs docked at the plasma membrane contribute preferentially to the first phase of insulin secretion (28). Mobilization of more distal insulin SGs is critical instead to sustain the second phase of insulin secretion. This model has been challenged by the detection of insulin SGs that crash and fuse with the plasma membrane immediately after their appearance in the TIRF microscopy field (29). As these "newcomer" insulin SGs contribute to both insulin secretory phases and newly synthesized insulin is preferentially released, it is of great interest to gain insight into the age distribution of "docked" and "newcomer" insulin SGs. Progress in this area, however, has been hampered by the lack of a method for the unequivocal time-resolved labeling of SGs. This approach has now been developed by tagging insulin with the SNAP tag (17–19). This technology has several advantages. It allows for the conditional labeling of targets with probes

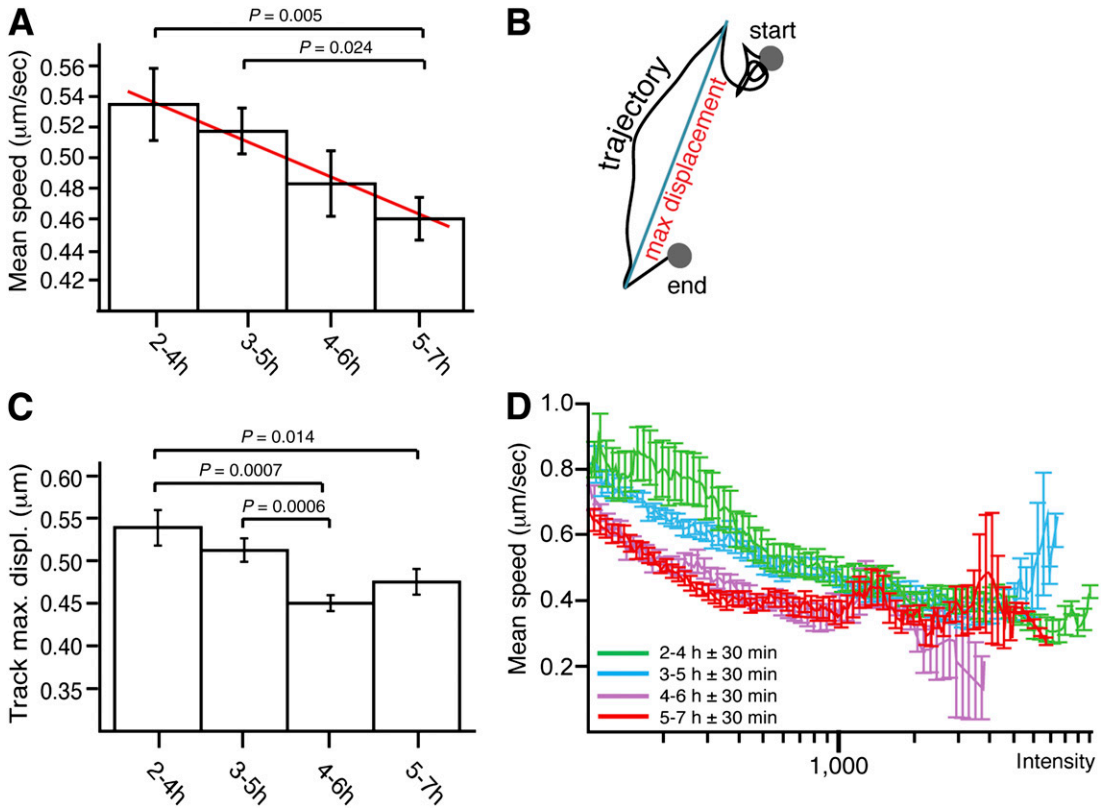

FIG. 4. Mobility and processivity of insulin SGs are age-dependent. TMR-Star–labeled *hIns-SNAP* INS-1 cells were imaged by single-color TIRF microscopy. Mobility and processivity of cortical insulin SGs were analyzed using the Motion Tracking software. The data shown in *A*, *C*, and *D* originated from the analysis of 20,369 tracks in total (results from 2–4 independent experiments are expressed as mean ± SEM). *A*: Mean speed of processive, age-distinct insulin SGs. The red straight line shows the maximum likelihood fit. The mean speed decay coefficient was −0.0266 ± 0.0079 μm/s/h. *y*-axis: mean speed. *B*: Illustration of the maximum displacement of SGs. *C*: Track maximum (max.) displacement (displ.) of processive, age-distinct insulin SGs. *y*-axis: track maximum displacement. *D*: Distribution of mean speed vs. intensity of processive, age-distinct insulin SGs. *y*-axis: mean speed.

suited not only for live cell imaging but also for affinity purification, thus greatly extending the range of feasible analyses compared with the classical radioisotope-based pulse-chase approach. Unlike approaches based on fluorescent proteins, including the "timer" reporter Ds-Red (30), it also enables the setting of accurate experimental time boundaries without resorting to photo bleaching, activation, or conversion. Being spatially restricted and potentially detrimental to cells, the latter approaches are inadequate for following the dynamics of entire populations of organelles such as insulin SGs.

The choice of insulin as reporter was favorable, being the most abundant cargo in β-cell SGs. Its employment together with SNAP was not obvious, since the latter relies on the reactivity of a cysteine with the substrate. As cysteines of secretory proteins are oxidized, ProIns-SNAP could have all been degraded in the endoplasmic reticulum, conjugated to other secretory proteins via disulphide bridges with free cysteines, or mistargeted as reported for insulin green fluorescent protein in some (31), albeit not all, cases (32). As ProIns-SNAP is converted less efficiently than endogenous proinsulin, its folding may indeed be altered in part. Accordingly, preliminary evidence suggests that glucose tolerance in SOFIA mice is impaired. Our data, however, indicate also that a fraction of Ins-SNAP is correctly processed, sorted into, and released from SGs.

The approach presented here allowed for the first time the simultaneous imaging of insulin SG pools with distinct and precisely defined ages. In principle, the number of age-distinct SG pools that may be visualized is only limited by

TABLE 3
Age-dependent changes of SG mean speed and track maximum displacement

Age (h)	Mean speed (μm/s)	*P*	Track maximum displacement (μm)	*P*
2–4	0.53 ± 0.023	vs. 5–7 h, 0.005	0.53 ± 0.020	vs. 5–7 h, 0.014; vs. 4–6 h, 0.0007
3–5	0.51 ± 0.015	vs. 5–7 h, 0.024	0.51 ± 0.013	vs. 2–4 h, 0.0007; vs. 4–6 h, 0.0006
4–6	0.48 ± 0.021	—	0.45 ± 0.009	vs. 3–5 h, 0.0006
5–7	0.45 ± 0.013	vs. 2–4 h, 0.005; vs. 3–5 h, 0.02	0.47 ± 0.015	vs. 2–4 h, 0.014

Images of TMR-Star$^+$ SGs ages 2–4, 3–5, 4–6, and 5–7 h were acquired by TIRF microscopy and the data analyzed for calculation of the mean speed and track maximum displacement of processive granules.

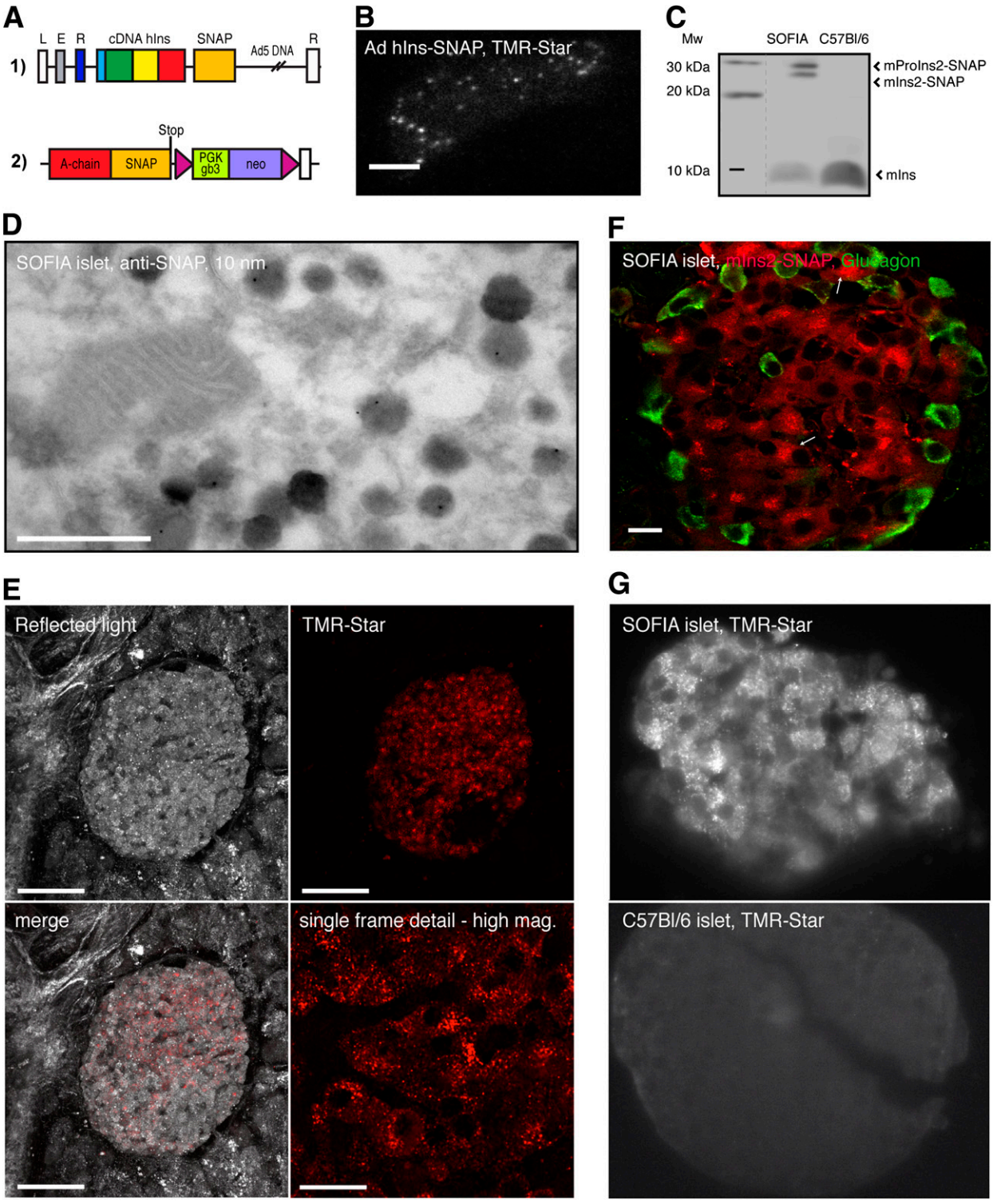

FIG. 5. Expression of Ins-SNAP in mouse islets in vitro and in vivo. *A*: *1*. Scheme of hIns-SNAP adenoviral vector. L, left inverted terminal repeats (white); E, encapsidation signal (gray); R (dark blue), rat insulin promoter. Light blue, signal peptide; green, B-chain; yellow, C-peptide; red, A-chain; orange, SNAP. R (white), right inverted terminal repeats. *2*. Scheme of the targeted *INS-2* locus in ESs prior to the removal of the region between the two flippase recognition target sites (magenta arrowheads); neo (purple), neomycin resistance. *B*: TIRF microscopy image of a single cell dissociated from mouse islets, infected with the hIns-SNAP adenoviral vector and labeled with TMR-Star. Scale bar: 5 μm. *C*: Immunoblot with the anti-insulin antibody on nonreduced extracts of islets isolated from *mIns-SNAP*$^{+/-}$ SOFIA and C57BL/6 mice. *D*: Cryoimmunoelectron microscopy of pancreatic islets isolated from SOFIA mice and immunolabeled with the mouse anti-SNAP antibody, followed by rabbit anti-mouse IgG and 10 nm gold particle–conjugated protein A. Scale bar: 500 nm. *E*: Confocal image (maximum-intensity projection) of a pancreatic tissue slice from a SOFIA mouse intravenously injected with TMR-Star. *Bottom left panel*: merge of images acquired by laser backscatter (*top left panel*) and fluorescence (*top right panel*). Scale bar: 100 μm. *Bottom right panel*: High magnification single optical confocal plane of an islet within the pancreatic tissue slice. Scale bar: 20 μm. *F*: Confocal image of a pancreatic cryosection from a SOFIA mouse intravenously injected with TMR-Star. Immunolabeling with anti-glucagon antibody. Scale bar: 10 μm. Arrows point to the region of the *trans*-Golgi network. *G*: Light-sheet microscopy imaging (single focal planes) of isolated islets from SOFIA (*top panel*) and C57Bl/6 (*bottom panel*) mice intravenously injected with TMR-Star. Scale bar: 50 μm. mag., magnification; Mw, molecular weight markers.

the availability of SNAP fluorescent substrates with distinct spectra. From a biological perspective, we could exclude that greater release of newly synthesized insulin reflects heterogeneity of cells with regard to their biosynthetic and secretory responsiveness, hence providing formal evidence in support of the original claim that younger SGs undergo preferential exocytosis. We could also show that insulin SGs located in proximity to the plasma membrane markedly decrease their speed and processivity as they age from 2 to 7 h—an early time point considering a half-life of ~30 h. This phenomenon may result from age-dependent changes in the coupling of insulin SGs to motors or competence for association with the cortical cytomatrix. Rab27a and its interacting proteins granuphilin and MyRIP/Slac2/Exophilin8 (33) as well as β2-syntrophin (34) may restrict the mobility of insulin SGs. Hence, it will be important to determine whether these or other factors change their association with insulin SGs overtime.

The release of an age-defined pool of TMR-Star$^+$ InsSNAP from INS-1 cells cultured in 384-well plates could be measured with fluorimetry. Implementation of this approach may therefore enable the development of high-throughput screenings for compounds differentially affecting the exocytosis of age-distinct insulin SGs. InsSNAP viral vectors and the SOFIA mouse, in turn, represent valuable tools to compare the turnover of insulin SGs in nondiabetic and diabetic human islets and mouse models.

ACKNOWLEDGMENTS

This work has been supported with funds from the German Ministry for Education and Research to the German Centre for Diabetes Research (http://www.dzd-ev.de) and the European Community's Seventh Framework Programme (FP7/2007-2013) for the Innovative Medicine Initiative under grant agreement no. 115005 (http://www.imidia.org). A.I. has been supported with a MedDrive grant from the Medical Faculty at Technical University Dresden.

No potential conflicts of interest relevant to this article were reported.

A.I. performed most of the experiments, analyzed data, and wrote the manuscript. Y.K. developed the MotionTracking software and performed statistical analysis of imaging data. R.D. measured insulin-SNAP by fluorimetry. M.Sa. helped in the generation of the targeting cassette generation. M.G. imaged islets in vibratome tissue slices. B.S.-D. provided assistance with TIRF microscopy. A.M. generated immunoelectron microscopy data. Y.L. transduced human islets with adenoviral vector. C.A. performed the 384-well plate assays. B.M. provided assistance with statistical analysis of TIRF microscopy data. C.M. isolated rodent islets. T.K. collaborated for immunoelectron microscopy experiments. M.B. supervised the 384-well plate assays and performed the segmentation analyses. S.S. supervised imaging of islets in vibratome tissue slices. K.A. provided expertise for the generation of the knock-in mice. M.So. conceived the project, analyzed data, and wrote the manuscript. M.So. is the guarantor of this work and, as such, had full access to all the data in the study and takes responsibility for the integrity of the data and the accuracy of the data analysis.

The authors thank C. Wollheim (University of Geneva) for the gift of INS-1 cells; Dr. J. Miyazaki (University of Osaka) and Dr. S. Seino for the gift of MIN6 cells; A. Brecht (Covalys) for providing SNAP reagents; R. Naumann (Max Planck Institute for Molecular Cell Biology and Genetics [MPI-CBG]) for help with the generation of transgenic mice; D. Krastev (MPI-CBG), J. Schindelin (MPI-CBG), and D. White (MPI-CBG) for discussions; P. De Camilli (Yale University, New Haven, CT) and M. Zerial (MPI-CBG) for reading of the manuscript; A. Altkrueger (Paul Langerhans Institute Dresden [PLID]), I. Baer (Center for Regenerative Therapies Dresden [CRTD]), S. Kretschmar (CRTD), K. Saydaminova (PLID), D. Richter (PLID), and A. Friedrich (PLID) for technical help; M. Chernykh (MPI-CBG) for MT software assistance; and K. Pfriem (PLID) for administrative help. The authors thank the Zentrum für Informationsdienste und Hochleistungsrechnen at Technical University Dresden for providing resources on their Deimos PC cluster.

REFERENCES

1. Gold G, Gishizky ML, Grodsky GM. Evidence that glucose "marks" beta cells resulting in preferential release of newly synthesized insulin. Science 1982;218:56–58
2. Halban PA. Differential rates of release of newly synthesized and of stored insulin from pancreatic islets. Endocrinology 1982;110:1183–1188
3. Sarov M, Schneider S, Pozniakovski A, et al. A recombineering pipeline for functional genomics applied to Caenorhabditis elegans. Nat Methods 2006; 3:839–844
4. Gotoh M, Maki T, Kiyoizumi T, Satomi S, Monaco AP. An improved method for isolation of mouse pancreatic islets. Transplantation 1985;40:437–438
5. Asfari M, Janjic D, Meda P, Li G, Halban PA, Wollheim CB. Establishment of 2-mercaptoethanol-dependent differentiated insulin-secreting cell lines. Endocrinology 1992;130:167–178
6. Miyazaki J, Araki K, Yamato E, et al. Establishment of a pancreatic beta cell line that retains glucose-inducible insulin secretion: special reference to expression of glucose transporter isoforms. Endocrinology 1990;127: 126–132
7. Trajkovski M, Mziaut H, Altkrüger A, et al. Nuclear translocation of an ICA512 cytosolic fragment couples granule exocytosis and insulin expression in beta-cells. J Cell Biol 2004;167:1063–1074
8. Kranz A, Fu J, Duerschke K, et al. An improved Flp deleter mouse in C57Bl/6 based on Flpo recombinase. Genesis 2010;48:512–520
9. Speier S, Rupnik M. A novel approach to in situ characterization of pancreatic beta-cells. Pflugers Arch 2003;446:553–558
10. Tokuyasu KT. A technique for ultracryotomy of cell suspensions and tissues. J Cell Biol 1973;57:551–565
11. Tokuyasu KT. Immunochemistry on ultrathin frozen sections. Histochem J 1980;12:381–403
12. Slot JW, Geuze HJ. Cryosectioning and immunolabeling. Nat Protoc 2007; 2:2480–2491
13. Costes SV, Daelemans D, Cho EH, Dobbin Z, Pavlakis G, Lockett S. Automatic and quantitative measurement of protein-protein colocalization in live cells. Biophys J 2004;86:3993–4003
14. Kalaidzidis Y. Multiple objects tracking in fluorescence microscopy. J Math Biol 2009;58:57–80
15. Collinet C, Stöter M, Bradshaw CR, et al. Systems survey of endocytosis by multiparametric image analysis. Nature 2010;464:243–249
16. Kalaidzidis YL, Gavrilov AV, Zaitsev PV, Kalaidzidis AL, Korolev EV. PLUK-an environment for software development. Program Comput Soft 1997;23: 206–212
17. Keppler A, Pick H, Arrivoli C, Vogel H, Johnsson K. Labeling of fusion proteins with synthetic fluorophores in live cells. Proc Natl Acad Sci USA 2004;101:9955–9959
18. Keppler A, Arrivoli C, Sironi L, Ellenberg J. Fluorophores for live cell imaging of AGT fusion proteins across the visible spectrum. Biotechniques 2006;41:167–170, 172, 174–175
19. Tirat A, Freuler F, Stettler T, Mayr LM, Leder L. Evaluation of two novel tag-based labelling technologies for site-specific modification of proteins. Int J Biol Macromol 2006;39:66–76
20. Orci L, Ravazzola M, Amherdt M, Madsen O, Vassalli JD, Perrelet A. Direct identification of prohormone conversion site in insulin-secreting cells. Cell 1985;42:671–681
21. Steiner DF, Michael J, Houghten R, et al. Use of a synthetic peptide antigen to generate antisera reactive with a proteolytic processing site in native human proinsulin: demonstration of cleavage within clathrin-coated (pro) secretory vesicles. Proc Natl Acad Sci USA 1987;84:6184–6188

22. Ehrhart M, Grube D, Bader MF, Aunis D, Gratzl M. Chromogranin A in the pancreatic islet: cellular and subcellular distribution. J Histochem Cytochem 1986;34:1673–1682
23. Bolte S, Cordelières FP. A guided tour into subcellular colocalization analysis in light microscopy. J Microsc 2006;224:213–232
24. Guest PC, Arden SD, Rutherford NG, Hutton JC. The post-translational processing and intracellular sorting of carboxypeptidase H in the islets of Langerhans. Mol Cell Endocrinol 1995;113:99–108
25. Liu M, Hodish I, Rhodes CJ, Arvan P. Proinsulin maturation, misfolding, and proteotoxicity. Proc Natl Acad Sci USA 2007;104:15841–15846
26. Malaisse-Lagae F, Amherdt M, Ravazzola M, et al. Role of microtubules in the synthesis, conversion, and release of (pro)insulin. A biochemical and radioautographic study in rat islets. J Clin Invest 1979;63:1284–1296
27. Porte D Jr. Banting lecture 1990. Beta-cells in type II diabetes mellitus. Diabetes 1991;40:166–180
28. Rorsman P, Renström E. Insulin granule dynamics in pancreatic beta cells. Diabetologia 2003;46:1029–1045
29. Shibasaki T, Takahashi H, Miki T, et al. Essential role of Epac2/Rap1 signaling in regulation of insulin granule dynamics by cAMP. Proc Natl Acad Sci USA 2007;104:19333–19338
30. Duncan RR, Greaves J, Wiegand UK, et al. Functional and spatial segregation of secretory vesicle pools according to vesicle age. Nature 2003;422:176–180
31. Pouli AE, Kennedy HJ, Schofield JG, Rutter GA. Insulin targeting to the regulated secretory pathway after fusion with green fluorescent protein and firefly luciferase. Biochem J 1998;331:669–675
32. Ohara-Imaizumi M, Nakamichi Y, Tanaka T, Ishida H, Nagamatsu S. Imaging exocytosis of single insulin secretory granules with evanescent wave microscopy: distinct behavior of granule motion in biphasic insulin release. J Biol Chem 2002;277:3805–3808
33. Kasai K, Fujita T, Gomi H, Izumi T. Docking is not a prerequisite but a temporal constraint for fusion of secretory granules. Traffic 2008;9:1191–1203
34. Schubert S, Knoch K-P, Ouwendijk J, et al. β2-Syntrophin is a Cdk5 substrate that restrains the motility of insulin secretory granules. PLoS ONE 2010;5:e12929